Nanoscale

Cite this: *Nanoscale*, 2012, **4**, 5588

www.rsc.org/nanoscale

COMMUNICATION

Multiferroic nanoscale Bi_2FeCrO_6 material for spintronic-related applications†

R. Nechache,*[ab] C. Harnagea[b] and F. Rosei[b]

Received 7th June 2012, Accepted 10th July 2012
DOI: 10.1039/c2nr31429k

We report the control of the growth mode of Bi_2FeCrO_6 thin and ultrathin films by either tuning the pulsed laser deposition parameters or by using a buffer layer. The films are epitaxial and the heterostructures exhibit very smooth interfaces, thus eliminating the main obstacle in the realization of tunnel junctions. By characterizing the functional properties of thin films we find that Bi_2FeCrO_6 retains its room temperature multiferroic character even at the nanoscale. The coexistence of these properties in ultra-thin Bi_2FeCrO_6 films will pave the way to design multifunctional devices for applications in spintronics and electronics, such as ferroelectric tunnel junctions or magnetic tunnel junctions with ferroelectric barriers.

The discovery of multifunctional materials exhibiting several properties simultaneously is the driving force behind continued scientific progress across several disciplines. Due to their highly tunable physical and chemical properties, complex oxides offer opportunities to realize new emergent phenomena that could not only challenge our current fundamental understanding but also provide real solutions for technological advances. In this context, multiferroic materials which combine two or more ferroic functionalities are promising for applications in fields such as spintronics and non-volatile data storage.[1,2] The integration of such materials in memory devices, for example, will yield an additional degree of freedom, enabling electrical writing and non-destructive magnetic reading processes. Ferromagnetic (ferroelectric) materials have a switchable spontaneous magnetization (polarization) and have already demonstrated their potential for data storage applications where the binary, non-volatile, information is stored in the two magnetization (polarization) states.[3] Combining the best functionalities of magnetic and ferroelectric memories (*i.e.* fast magnetic, non-destructive read and ferroelectric writing) in the same device will lead to the design of a non-volatile and robust memory device with enhanced processing speeds and reduced energy consumption. In this context, MF materials[4,5] offer a promising new alternative to achieve the "ultimate memory device"[6] by adding logic states while reducing device dimensions. As recently demonstrated[7] ferromagnetic–ferroelectric $La_{0.1}Bi_{0.9}MnO_3$ can be advantageously used as a barrier in a multiferroic tunnel junction (MFTJ) to independently encode the information in electric polarization and magnetization giving rise to a four state logic memory. On the other hand, a coupling between magnetic and electrical properties would lead to additional degrees of freedom for related devices, such as electric field-controlled magnetic data storage.[8–10] The recent emergence of Bi-based double perovskite thin films, such as Bi_2FeCrO_6 (BFCO)[11–14] and Bi_2CoMnO_6,[15] with strong MF behaviour at room temperature, creates opportunities to use MFs in real applications. This requires (1) the stability of both ferroelectricity and magnetic properties for a very thin tunnel barrier and (2) good interface properties such as stoichiometry, smoothness and crystallinity in the multilayered heterostructure, which are usually involved in such multijunctions. These critical factors can significantly affect MFTJ performance, in terms of tunnel electroresistance (TER) or tunnel magneto-resistance (TMR), seriously limiting their use in devices. Theoretical and experimental reports revealed that these requirements can be achieved in perovskite oxides, in which ferroelectricity[16–18] and magnetism[7] persist in nanoscale thin films.

In a previous study,[13] we analyzed the effect of the oxygen deposition pressure and substrate temperature on the properties of epitaxial 90 nm thick BFCO grown by pulsed laser deposition (PLD), directly on single crystalline Niobium doped $SrTiO_3$ (STO:Nb) substrates. We have found a narrow window for which the films are phase-pure, within the limits of X-ray diffraction and photoemission spectroscopy. Later, we established that the quality of the films also depends on the substrate and, more importantly, their magnetization depends on their thickness, with thinner films exhibiting a stronger magnetic response, and we associated this dependence with the degree of cationic order, which decreases as the films are grown thicker.[19]

Here we report the properties of epitaxial BFCO thin and ultrathin films with a thickness between 2 and 20 nm. We managed to control the epitaxial growth mode of the films using vicinal 100-oriented STO:Nb substrates. We also show that the layer-by-layer growth mode is stabilized when using $SrRuO_3$ (SRO) as buffer layer. We study the morphological, structural, electrical, and magnetic properties of these very thin BFCO/SRO bilayers, and we demonstrate that this heterostructure exhibits a negative exchange bias only below the ferromagnetic Curie temperature of the SRO layer. We show that the RT magnetic and ferroelectric properties of BFCO are preserved

[a]*NAST Center & Department of Chemical Science and Technology, University of Rome Tor Vergata, Via della Ricerca Sceintifica 1, 00133 Rome, Italy. E-mail: nechache@emt.inrs.ca*
[b]*Centre Énergie, Matériaux et Télécommunications, INRS, 1650, boulevard Lionel-Boulet, Varennes, Québec J3X 1S2, Canada*
† Electronic supplementary information (ESI) available. See DOI: 10.1039/c2nr31429k

at the nanoscale, thus satisfying the essential criteria for being used as multiferroic tunnel barriers.

The BFCO and the bottom electrode SRO thin films were grown by PLD at substrate temperatures and oxygen partial pressures ranging between 600–680 °C and 5–100 mTorr. The laser fluence and laser repetition rate were varied from 1 to 2 J cm^{-2} and 2 to 8 Hz, respectively with respect to the desired growth mode for the deposited layers. The films were grown on (100)-oriented STO single crystalline substrates with vicinal terraces 100 to 250 nm in width.

The substrates were prepared by dipping the as-received STO in buffered hydrofluoric acid for 30 s, followed by thermal annealing at 950–1100 °C for 10 min, yielding single-unit-cell stepped surfaces with TiO_2-termination (*cf.* Fig. 1a).

To investigate the early stages of the growth mode of these different materials, the surface morphology of the as-grown films was studied by atomic force microscopy (AFM) in tapping mode.

Fig. 1a shows a perfect TiO_2-terminated surface of (100) STO substrate. One can clearly see step-terrace structures with a height of only one unit cell. The control of the early stage growth mode of BFCO on such a STO surface is shown in Fig. 1b and c: depending on the growth conditions, BFCO adopts either a 3D (islands, Volmer–Weber) or 2D (layer-by-layer, Frank-van der Merwe) growth mode. When the film is deposited at a growth rate of 0.5 Å s^{-1}, 680 °C, $p_{O2} = 8$ mTorr, islands nucleate on STO terraces, the surface roughness being higher than the step (Fig. 1b). A grainy BFCO layer (with an average grain size and height of 14 nm and 0.57 nm, respectively) uniformly covers the substrate, with the terrace steps barely being visible. By slightly modifying the PLD conditions, *i.e.* growth at 600 °C, $p_{O2} = 4$ mTorr and a growth rate of 0.13 Å s^{-1}, the BFCO layer uniformly covers the STO terraces (*cf.* Fig. 1c).

The layer-by-layer growth regime was also achieved for thicker films up to at least 35 nm, provided that the substrate surface is clean enough and well prepared. In this regime, since the substrate strongly influences the growing microstructure, the coherent, epitaxial growth prevails.[20] In our case the width of the STO terraces is rather critical, since under the same PLD conditions, we observed a different growth mode for BFCO. This phenomenon has been previously observed and an empirical model has been established.[21]

According to the classical theory of film nucleation and growth, the selection of the growth modes by a specific substrate-film system depends on thermodynamics, *i.e.* on the surface energies of both film and substrate, and on the film–substrate interface energy.[22] A typical scenario of film growth is the following:[23] when diffusing ad-atoms encounter a step edge, they can either be reflected and remain on the same terrace, or cross the terrace and be incorporated into sites at the terrace edges. If all the terraces are non-reflective for the diffusing ad-atoms or clusters, the growth process will be 2D, because atoms will attach to the edges of the terraces where their energy is minimum. Alternatively, if the terraces are reflective, the atoms diffuse on the terraces finally covering the entire surface with a very thin uniform layer resulting in 3D growth mode.

In our case, the initial STO surface roughness is 0.13 nm, while after depositing 2.5 nm of BFCO in the 3D growth mode the roughness increases to 0.83 nm, indicating a rough top-surface of the BFCO layer. In contrast, the surface morphology of BFCO films grown layer-by-layer exhibits clear terraces with a step height close to the perovskite lattice cell (0.414 nm) and a low roughness (rms = 0.17 nm). The same morphology is obtained when BFCO is grown on SRO-buffered STO (100) substrates (Fig. 2b). The SRO buffer layer grows atomically flat (rms = 0.15 nm), with one-unit-cell stepped terraces (step-flow growth regime) (*cf.* Fig. 2a), following the terraces of the vicinal STO substrate (Fig. 1a).[23] The surface of the bilayer BFCO (18 nm)/SRO (15 nm) is relatively smoother (rms = 0.19 nm) compared to that of the 3D-grown BFCO deposited, under the same conditions, directly on the STO substrate (*cf.* Fig. 1b and 2b). The growth mode is 2D in both cases, with BFCO ad-atoms apparently nucleating at SRO step edges and following the terrace's topography. Since the in-plane lattice parameter of SRO/STO and STO is the same (~0.39 nm), the difference in film morphology in the two cases cannot result from different elastic energies, but rather due to the difference of the surface energies of the SRO buffer layer and substrate. This 2D morphology and low roughness make BFCO layers suitable for application in tunnel junction devices. The BFCO/SRO heterostructure has a peak-to-peak roughness much lower than the typical thickness of the tunnel barrier and thus limits the short-circuit effect in the device.

High resolution transmission electron microscopy confirms the epitaxial growth of the heterostructure with sharp and well-defined interfaces (not shown here). The "orange peel" effect usually observed in irregular layers will also probably be restricted. Furthermore, the correct chemical stoichiometry of materials comprising the heterostructure is revealed by combined Rutherford backscattering spectrometry (RBS) and Elastic Recoil Detection (ERDA) analysis (data not shown here).

To assess the ferroelectric properties of our ultrathin films we used two variants of scanning force microscopy with voltage modulation:

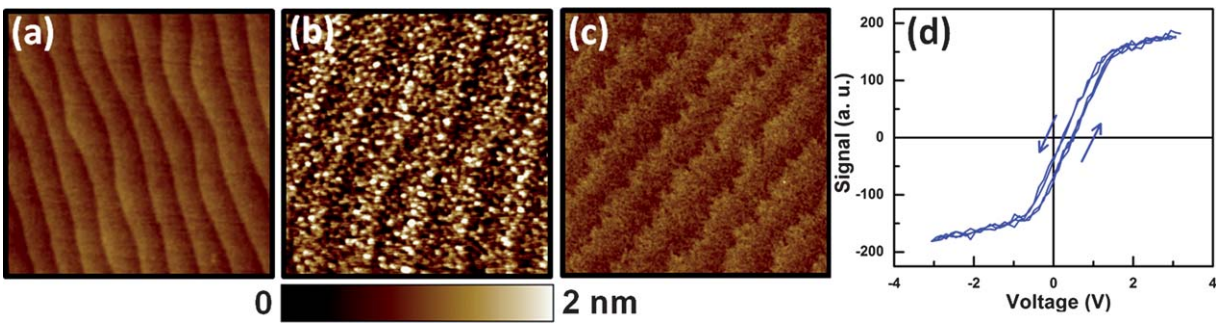

Fig. 1 (a) AFM images (2 μm × 2 μm) of a vicinal STO substrate obtained after adequate surface treatment showing one-unit-cell stepped terraces (~200 nm wide). (b and c) Control of the growth mode of BFCO ultrathin (2.5 nm thick) films grown directly on STO vicinal surfaces: 3D (islands) growth mode achieved at a substrate temperature of 680 °C (b) and 2D growth (layer-by-layer), at 600 °C (c). (d) Open-loop Kelvin probe measurement proving the switching of polarization, thus ferroelectricity.

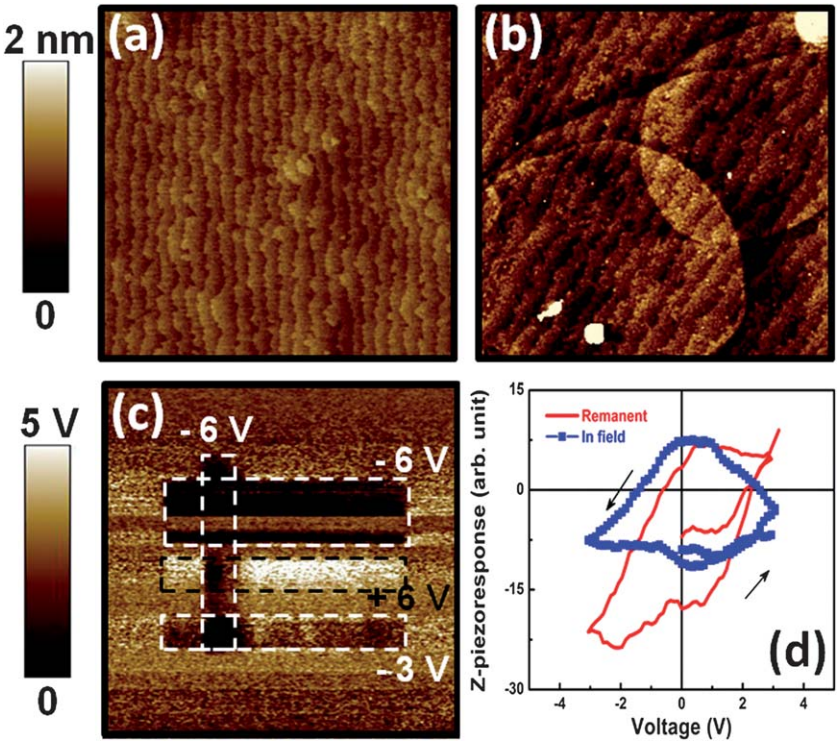

Fig. 2 (a) Typical morphology of the SRO step-flow growth (film thickness 15 nm) on TiO_2-terminated surface of (100) STO substrate. (b) AFM image (5 μm × 5 μm) of 18 nm-thick BFCO film grown on SRO/STO. (c) z-PFM image of the heterostructure showing induced ferroelectric polarization: black/white contrast corresponds to a negative/positive bias previously applied to the substrate. (d) Local z-PFM hysteresis loops (in Field and remanent).

open-loop Kelvin Probe Microscopy (OL-KPM)[24,25] and Piezoresponse Force Microscopy (PFM). In these techniques, an ac-voltage is applied between the conductive tip of the AFM and the bottom electrode (here substrate) of the sample. The ac voltage has to be below the coercive field of the sample, such that it does not induce polarization switching, and thus the signal detected contains only polarization information. In PFM, the AFM tip that is in contact with the sample transmits the piezoelectrically induced vibration to the supporting cantilever, and the signal represents the sample electromechanical response, proportional to the sample polarization. Because the coercive field of BFCO is about 400 kV cm^{-1} (ref. 13) for ultrathin films (2.5 nm) this corresponds to a maximum ac voltage of 100 mV, which proved to be insufficient to obtain a measurable PFM signal. Therefore, to alleviate noise problems, we used OL-KPM, in which the surface potential under the tip (dependent on the polarization in the sample) induces a cantilever vibration.[26] Being a non-contact method, the field applied to the sample is lower than that for PFM, while the polarization signal, originating in the electrostatic interaction, is strong enough. In Fig. 1d we show an OL-KPFM hysteresis loop obtained for a BFCO ultrathin film which confirms the ferroelectric character. The shift of the hysteresis loop towards positive bias can be linked to several factors, among which are domain pinning[27] and rectifying effects formed at the ferroelectric-electrode interface,[28] well known size effects usually observed when the characteristic size of ferroelectric structures is reduced. Similarly, the hysteresis loop of the bilayer (Fig. 2d) exhibits a shift along the polarization axis, suggesting an imprint of polarization towards the substrate.

The investigation of magnetic coupling in the BFCO/SRO structure is essential to understand the factors affecting the rotation of their spins and evaluate the use of BFCO in magnetic tunnel junctions. To assess the magnetization coupling in the heterostructure, we compare the magnetic behavior of the BFCO/SRO/STO heterostructure to that of a BFCO/STO film with a very similar thickness.

At the interface between two magnetic materials the exchange interaction between spins at the interface is dominant and can dramatically change the magnetic response of the whole heterostructure. Macroscopic magnetic hysteresis loops were measured with a superconducting quantum interference device (SQUID) magnetometer from Quantum Design (sensitivity: 5×10^{-8} emu at low temperature). Fig. 3 shows magnetization hysteresis curves for the as-grown films that demonstrate the existence of an exchange bias in the BFCO/SRO/STO heterostructure. After being cooled in a magnetic field of 500 Oe applied parallel to the interface, its hysteresis loop is shifted along the field axis. The magnetic hysteresis loops were measured by sweeping the magnetic field between ±6 kOe parallel to the sample surface. Here we only show minor loops between ±2 kOe: a field sufficient to fully switch magnetization in the BFCO but far below the coercive field of the SRO layer. Cooling the sample in a positive magnetic field along a certain direction results in a negative shift of the hysteresis loop of the heteroepitaxial BFCO/SRO/STO bilayer towards the opposite direction (*cf.* Fig. 3b).

The coercive field (H_C), which is defined as half the width of the hysteresis loop ($H_{C+} - |H_{C-}|$)/2, is found to be 180 Oe. The exchange bias H_{EB} (equal to the shift of the center of the loop ($H_{C+} + |H_{C-}|$)/2) is 72 Oe at 10 K. The magnetic hysteresis loop of the BFCO/STO structure shows a lower H_c (= 100 Oe) and, more importantly, a symmetric hysteresis loop, even though it has been cooled down in the same magnetic field as the BFCO/SRO/STO heterostructure. The large anisotropy and its high coercive field make SRO a good

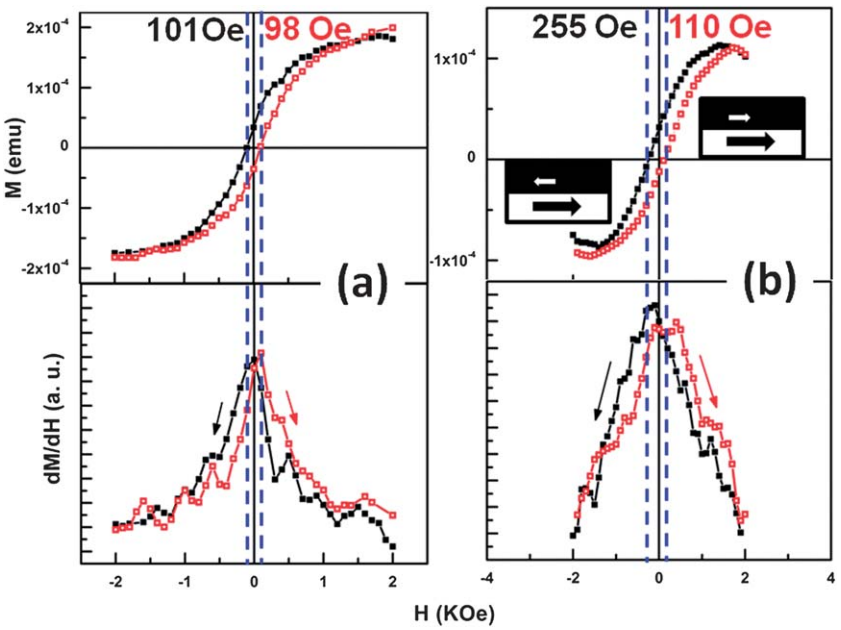

Fig. 3 Magnetic hysteresis curves of (a) BFCO/STO:Nb and (b) BFCO/SRO/STO:Nb heterostructures obtained from SQUID measurements made at 10 K. The curves were measured after the samples had been field-cooled from 400 K in 500 Oe. A negative shift of the hysteresis loop is observed for the BFCO/SRO/STO structure, while a symmetric hysteresis characterizes BFCO/STO film. Derivative of the curves are also shown in the bottom panel.

candidate for use as a biasing layer.[29] The Curie temperature (T_C) of SRO being around 150–160 K also allows us to conveniently study the bias exchange effect above and below the T_C of the biasing layer. Our measurements confirmed the value of the T_C (~160 K, data not shown). On the other hand, since BFCO has a low coercivity and a T_C higher than that of SRO, the BFCO/SRO bilayer epitaxial heterostructure is a potential candidate for use in multiferroic tunnel junctions.[13,30] When BFCO is coherently and epitaxially grown on top of ferromagnetic SRO the exchange coupling across the interface between the two systems leads to: (1) an increased coercivity of BFCO from 100 Oe to 180 Oe (*cf.* Fig. 3). This is usually attributed to the increased coercivity of "interfacial spins" which need to be dragged around by the external field; (2) an asymmetry of the BFCO hysteresis loop, specifically a shift along the field axis, dependent on the magnetization induced previously in the biasing SRO layer (Fig. 3b). This unidirectional shift demonstrates a bias exchange interaction between the two layers, the magnetization of BFCO having a preferred magnetization orientation. The magnetization of BFCO is pinned by the ferromagnetic SRO into this direction. Further use of BFCO films as a barrier in spin valve structures will need an additional layer, insolating and non-magnetic, such as STO to avoid the magnetic coupling between the BFCO and the ferromagnetic electrode.

Conclusion

In summary, we demonstrated the control of the growth mode of BFCO thin and ultrathin films by either tuning PLD deposition parameters or by using a buffer layer. The films are epitaxial and the heterostructures exhibit very smooth interfaces, thus eliminating the principal obstacle in the realization of tunnel junctions. The investigation of the magnetic properties of the BFCO/SRO heterostructure revealed a magnetic coupling across the interface evidencing the presence of a bias-exchange field. The local piezoelectric measurements show that the ferroelectric character of BFCO persists even at nanoscale size (2.5 nm). The coexistence of these properties in the ultrathin BFCO films will pave the way to design novel device concepts for spintronic and electronic applications, such as ferroelectric tunnel junctions[31] or magnetic tunnel junctions with ferroelectric barriers. The investigation of magnetoresistance in such BFCO-based heterostructures is under work to evaluate its potential use in practical devices.

Acknowledgements

R.N. is grateful to the joint laboratory on Advanced Materials for Energy, Environment and Health, University of Rome "Tor Vergata" and INRS-EMT for partial salary support. R.N. and C.H. are grateful to NSERC financial support through personal fellowships. One of the authors (R.N.) wishes to thank Professor P. Fournier and M.-P. Singh from the University of Sherbrooke for SQUID measurements as well as A. Pignolet for fruitful discussions.

References

1 V. E. Wood and A. E. Austin, *Int. J. Magn.*, 1974, **5**, 303.
2 I. Zutic, J. Fabian and S. Das Sarma, *Rev. Mod. Phys.*, 2004, **76**, 323.
3 J. F. Scott and C. A. Paz de Araujo, *Science*, 1989, **246**, 1400.
4 H. Schmid, *Ferroelectrics*, 1994, **162**, 317.
5 G. A. Smolenskii and I. Chupis, *Sov. Phys. Usp.*, 1982, **25**, 475.
6 J. F. Scott, *Nat. Mater.*, 2007, **6**, 256.
7 M. Gajek, *et al.*, *Nat. Mater.*, 2007, **6**, 296.
8 N. Hur, S. Park, P. A. Sharma, J. S. Ahn, S. Guha and S. W. Cheong, *Nature*, 2004, **429**, 392.
9 T. Kimura, T. Goto, H. Shintani, K. Ishizaka, T. Arima and Y. Tokura, *Nature*, 2003, **426**, 55.
10 M. Fiebig, T. Lottermoser, D. Frohlich, A. V. Goitsev and R. V. Pisarev, *Nature*, 2002, **419**, 818.
11 R. Nechache, C. Harnagea, A. Pignolet, F. Normandin, T. Veres, L.-P. Carignan and D. Ménard, *Appl. Phys. Lett.*, 2006, **89**, 102902.

12 R. Nechache, C. V. Cojocaru, C. Harnagea, C. Nauenheim, M. Nicklaus, A. Ruediger, F. Rosei and A. Pignolet, *Adv. Mater.*, 2011, **23**, 1724.
13 R. Nechache, C. Harnagea, L.-P. Carignan, O. Gautreau, L. Pintilie, M. P. Singh, D. Menard, P. Fournier, M. Alexe and A. Pignolet, *J. Appl. Phys.*, 2009, **105**, 061621.
14 N. Ichikawa, M. Arai, Y. Imai, K. Hagiwara, H. Sakama, M. Azuma, Y. Shimakawa, M. Takano, Y. Kotaka, M. Yonetani, H. Fujisawa, M. Shimizu, K. Ishikawa and Y. Cho, *Appl. Phys. Express*, 2008, **1**, 101302.
15 M. P. Singh, K. D. Truong, P. Fournier, P. Rauwel, L. H. Carignan and D. Ménard, *Appl. Phys. Lett.*, 2008, **92**, 112505.
16 N. A. Spaldin, *Science*, 2004, **304**, 1606.
17 D. D. Fong, G. B. Stephenson, S. K. Streiffer, J. A. Eastman, O. Auciello, P. H. Fuoss and C. Thompson, *Science*, 2004, **304**, 1650.
18 H. Béa, *et al.*, *Jpn. J. Appl. Phys., Part 2*, 2006, **45**, L187.
19 R. Nechache, C. Harnagea and A. Pignolet, *J. Phys.: Condens. Matter*, 2012, **24**, 096001.
20 J. W. Matthews, *Epitaxial Growth Part B*, Academic, New York, 1975, ch. 4.
21 W. Hong, H. N. Lee, M. Yoon, H. M. Christen, D. H. Lowndes, Z. Suo and Z. Zheng, *Phys. Rev. Lett.*, 2005, **95**, 095501.
22 J. S. Horwitz and J. A. Sprague, in *Pulsed Laser Deposition of Thin Films*, ed. D. B. Chrisey and G. K. Hubler, Wiley, New York, 1994, p. 231.
23 D. B. Chrisey and G. T. T. Tsong, *Surface Diffusion- Atomistic and Collective Processes*, ed. M. C. Tringides, Plenum Press, New York, 1997, p. 49.
24 S. V. Kalinin and D. A. Bonnell, *Phys. Rev. B: Condens. Matter Mater. Phys.*, 2002, **65**, 125408.
25 T. Melin, M. Zdrojek and D. Brunel, Electrostatic Force Microscopy and Kelvin Force Microscopy as a Probe of the Electrostatic and Electronic Properties of Carbon Nanotubes, in *Scanning Probe Microscopy in Nanoscience and Nanotechnology*, ed. B. Bhushan, Springer-Verlag Berlin, Heidelberg, 2010, ch. 4.
26 In true KPM, this vibration is nullified by applying a bias equal (but with opposite sign) to the surface potential, by a Kelvin feedback loop.
27 D. Nagasawa and H. Nozawa, *Jpn. J. Appl. Phys., Part 1*, 1999, **38**, 5406.
28 Y. Xu, C. J. Chen, R. Xu and J. D. Mackenzie, *J. Appl. Phys.*, 1990, **67**, 2985.
29 Q. Gan, R. A. Rao, C. B. Eom, L. Wu and F. Tsui, *Appl. Phys. Lett.*, 1999, **85**, 5297.
30 S. Kamba, D. Nuzhnyy, R. Nechache, K. Zaveta, D. Niznansky, E. Santava, C. Harnagea and A. Pignolet, *Phys. Rev. B: Condens. Matter Mater. Phys.*, 2008, **77**, 104111.
31 J. Rodriguez Contreras, H. Kohlstedt, U. Poppe, R. Waser, C. Buchal and N. A. Pertsev, *Appl. Phys. Lett.*, 2008, **83**, 4595.

